IMPLEMENTATION AND EVALUATION OF AN ARTHROSCOPIC TRACKER SYSTEM FOR INTRAOPERATIVE MOTION TRACKING AND FORCE REGISTRATION

Øystein Bjelland
Lars Ivar Hatledal
Robin T. Bye

Cyber-Physical Systems Laboratory
Department of ICT and Natural Sciences
Norwegian University of Science and Technology
Larsgårdsveien 2, NO-6009 Ålesund, Norway
E-mail: oystein.bjelland, laht, robin.t.bye@ntnu.no

Martin Steinert

Trolllabs
Department of Mechanical and Industrial Engineering
Norwegian University of Science and Technology
Richard Birkelands vei 2B, NO-7491 Trondheim, Norway
E-mail: martin.steinert@ntnu.no

KEYWORDS

Digital Twin; Medical Simulation; Arthroscopy

ABSTRACT

This paper presents implementation and evaluation of an intraoperative arthroscopic tracker system for research and educational use. The system enables automatic pose and force data exchange between a physical asset and a digital model, which is required in arthroscopic digital twins. Surgical instrument motion tracking is captured using an inertial measurement unit in combination with stereo vision (ZED mini, Stereolabs, USA), and force registration is achieved using a 6 degree-of-freedom force-torque sensor (Nano 25, ATI Industrial Automation, USA). An integration layer in the software system continuously fetches data from the sensors, and transmits data over a network connection. The software visualization layer displays the instrument pose and force readings relative to a 3D anatomical model in real-time (24 Hz). Position accuracy of the system was compared to a Kuka LBR Med 14 R820 collaborative robot, and the total root mean square error was found to be 12.60 mm. A post-operative instrument trajectory map from sampled pose and force/torque data was implemented in Matlab, and demonstrated in an experiment. The system is considered feasible for use in many research and educational applications.

BACKGROUND

With more sensor data available nowadays, digital twins have recently gained much attention and is currently an active field of research. In healthcare, recent advances in automatic segmentation of magnetic resonance imaging (MRI) models using machine learning methods have enabled automatic creation of patient specific digital anatomical models in a short amount of time (Kulseng et al., 2023), which makes implementation of digital twins in clinical healthcare feasible. Many definitions have been proposed for digital twins in healthcare, mostly describing the patient as a physical system to be modelled (Lauzeral et al., 2019; Corral-Acero et al., 2020; Chase et al., 2021; Aubert et al., 2021; Hernigou et al., 2021; Bjelland, Rasheed, Schaathun, Pedersen, Steinert, Hellevik and Bye, 2022). Moreover, Fuller et al. (2020) describes that there must exist automatic data exchange between the physical system and the model, and that the flow of information must not only go from the physical asset to the digital twin, but also from the digital twin back to the physical asset. This separates a digital twin from a digital model. For arthroscopic knee surgery, recent efforts have focused on real-time patient-specific surgical simulation with kinesthetic haptic feedback for resident doctor training and pre-operative planning purposes. In this setting, some patient-specific simulations have been referred to as digital twins. However, we argue that for these simulation models to be considered a true digital twin, they must consider intraoperative data with automatic data exchange (Bjelland, Pedersen, Steinert and Bye, 2022), as shown in Fig. 1.

Intraoperative data collection can be classified into (i) force sensing techniques, and (ii) instrument tracking techniques for surgical navigation. Surgical interaction force measurements are often used in haptic research related to haptic rendering for surgical simulations in impedance based kinesthetic systems. Force measurements can be used in the simulation indirectly by calibrating a finite element material model by manual or automatic methods, or directly by interpolation methods, as described by Bjelland, Pedersen, Steinert and Bye (2022). Another application of surgical interaction force measurements is to provide force feedback during surgical training (not to be confused with kinesthetic haptic feedback), which can be beneficial for resident doctors. For example, a study showed that almost half of the errors made my novice surgeons were related to excessive use of force (Tang et al., 2005). Golahmadi et al. (2021) performed a systematic review of tool-tissue forces in surgery, and stated that force measurements can provide a quantitative metric of surgical skills, as well as allowing for definition and characterization of safe force ranges for specific maneuvers. They found that novices exerted 22.7% more force than experts, and that a force feedback mechanism (e.g. sound, visual or haptic) reduced interaction forces by 47.9%.

Surgical force sensing techniques can be categorized into direct and indirect methods. For direct methods, the force sensor is normally placed near or on the surgical instrument (Song and Fu, 2019). Measurement principles for multidimensional force sensors include resistive, capacitive, piezoelectric, optical fiber and strain gauge based principles. For indirect methods, the force sensors are placed between the
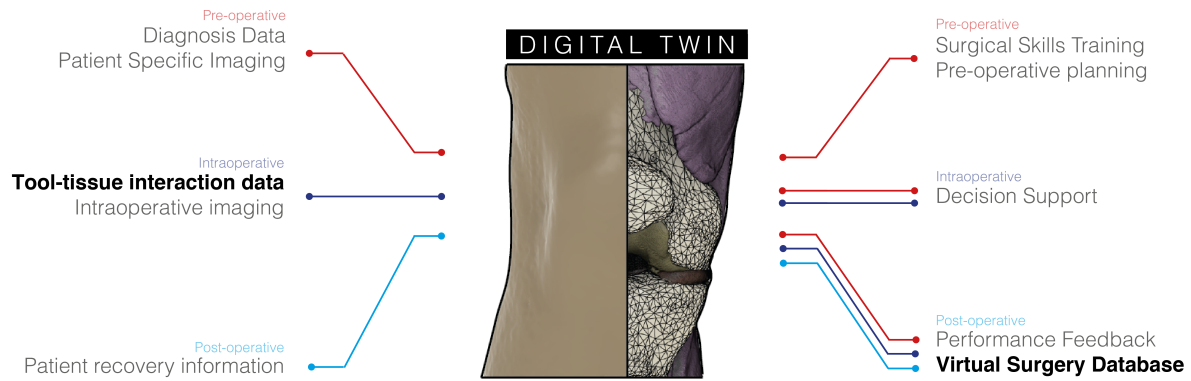
Fig. 1: Arthroscopic digital twin schematic for implementation of a system for collection of intraoperative tool-tissue interaction data, enabling intraoperative decision support and a post-operative virtual surgery database. Adapted from Bjelland, Pedersen, Steinert and Bye (2022).

patient and a static object. Because indirect methods could require more force sensors, and are more prone to bias from patient movement, direct methods are usually preferred. A recent review investigated image-based force estimation for medical applications, and found that these methods are now feasible for estimating interaction forces for providing haptic feedback in telerobotic systems (Nazari et al., 2021). However, the image-based methods rely on learning-based or model-based relations between force and deformation, and are thus not suitable for tissue characterization.

Instrument motion tracking enables enhanced intraoperative surgical navigation, with the goal of determining instrument pose (position and orientation) relative to patient-specific anatomy. It also enables detailed recording of the surgical tool-path, that can later be used to create a post-operative trajectory map or database. For instrument tracking in surgical navigation, the two most common commercially available techniques are based on optical or electromagnetic tracking. Optical tracking systems (OTS) normally use fiducial markers that can be attached to the instrument or anatomical structure, although recent efforts have demonstrated the use of markerless navigation (Hu et al., 2021). The position accuracy of recent optical systems has been found to be 0.045 mm (Fattori et al., 2021). The limitation of optical systems is that they need a direct line of sight between the camera and tool, and the tool tip position must therefore be estimated by the use of kinematic relations. Electromagnetic systems (EMTS) are based on small electromagnetic sensors that can be inserted on the tip of a surgical instrument. This allows for in-body tracking with a position and orientation accuracy of approximately 2.2 mm and 0.5° (Attivissimo et al., 2021). However, commercial electromagnetic systems have a limited work space of 500 mm, and the accuracy can be affected by the presence of ferromagnetic materials. Commercial systems can also be prohibitively expensive for lab research. Recent developments in low-cost stereo camera systems have made motion tracking more available to the general public. Recently, an arthroscopic tracking system based on an inertial measurement unit (IMU) in combination with stereo vision was

presented (Ma et al., 2020). This system utilized a ZED mini (Stereolabs, USA) stereo camera with a built in IMU sensor to replace external tracking systems, by estimating pose using visual-inertial stereo slam (VISS). This enables a much larger work space than traditional systems. The position accuracy of the system was compared with a high-end optical tracker system (Polaris, Northern Digital, Canada), and the mean square error between the two systems was found to be 0.99 mm.

This paper presents an arthroscopic tracker system for research and educational use. The system enables automatic pose and force data exchange between a physical asset and a digital model, which provides the foundation for an arthroscopic digital twin. Intraoperative motion tracking is achieved through a combination of stereo vision and IMU with 6 DOF, and force registration is achieved through a 6 DOF high-end force-torque sensor. This builds on previous work by Ma et al. (2020), but expands the system to include interaction force measurements. The system utilizes automatically segmented 3D-anatomic models obtained by MRI scans, which can create patient-specific models in a short amount of time (Kulseng et al., 2023). The functionality of the presented system includes:

- real-time intraoperative navigation support with patient-specific anatomy,
- real-time intraoperative force feedback through a visual feedback mechanism,
- synchronized tool-path and force-interaction database for haptic research, and a
- post-operative instrument trajectory map with forces.

The contributions of this paper can be summarized as:

- Hardware design and software implementation for an arthroscopic tracker system that enables automatic data exchange for arthroscopic digital twins.
- Implementation of a post-operative instrument trajectory map simulation.
- An evaluation experiment demonstrating the position accuracy of the system.
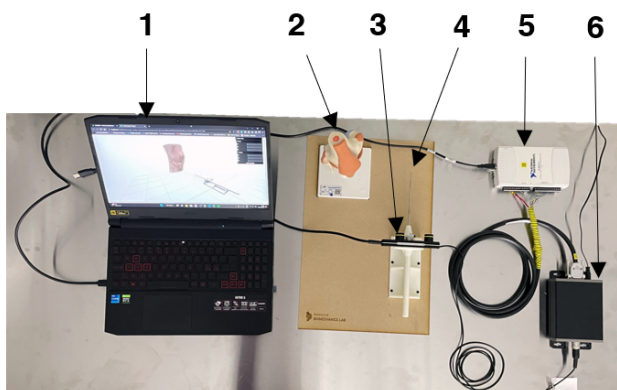
1. Windows PC with CUDA enabled GPU.
2. 3B functional knee model (#1000163).
3. Arthroscopic Tracker Assembly.
4. Laser cut MDF plate with 3D-printed tracker stand.
5. National Instruments myDAQ.
6. ATI DAQ Interface Power Supply.

Fig. 2: System overview with main system components.

SYSTEM DESCRIPTION

In the following, a description of the implemented prototype is given. The system consists of a hardware platform with just a few easy to move parts, as well as a distributed software package for sensory data collection, transmission and visualisation.

Hardware

The hardware system consists of a Windows PC, an arthroscopic tracker assembly, a laser cut MDF plate with a 3D-printed stand attached, a National Instruments (NI) myDAQ device, and an ATI DAQ interface power supply. An overview is shown in Fig. 2. A functional knee model from 3B scientific (no. 1000163) is included to represent the physical asset, and is used for demonstration purposes. The laser cut MDF plate ensures a fixed position between the knee model and the start position of the arthroscopic tracker prototype.

The arthroscopic tracker assembly consists of a modified Arthrex AR 10000 hook probe instrument for arthroscopic examination, a custom 3D-printed tool adapter, an ATI force-torque sensor, a ZED Mini stereo camera/IMU, a custom 3D-printed handle, and miscellaneous fasteners. The arthroscopic assembly is shown in Fig. 3. The AR 10000 hook probe is fastened to the tool adapter using a perpendicular M3 set screw. By interchanging the 3D-printed tool adapter, other surgical instruments can easily be fixed to the setup.

The force-torque sensor embedded in the arthroscopic device is a Nano25 multi-axis force/torque sensor system from ATI Industrial Automation (USA). The sensor, shown in Fig. 3, only weighs 0.0634 kg and is connected to a NI myDAQ device. The system measures all six components of force and torque, and consists of a transducer, shielded high-flex cable, and intelligent data acquisition system. The force-torque sensor is factory calibrated for a force of ±250 N in the perpendicular directions and 1000 N in the axial direction, with a measurement uncertainty less than 1% of its full scale load. By combining it with the arthroscopic device, it is possible to measure and record the force exerted by the tool during operation.

The ZED Mini, visible in Fig. 3, is a stereoscopic camera for spatial high-resolution image capture. It uses the images received from the two cameras to create a depth-map of the captured scene and can detect depth up to 15 meters. Additionally, it is equipped with both an accelerometer and a gyroscope for accurate spatial tracking. By attaching it to the arthroscopic device, its movements can be recorded during operation. The reported accuracy for 6 DOF pose from the product data sheet is ±1 mm for position, and $0.5°$ for orientation. The maximum sampling rate is 100 Hz.

As mentioned, both sensors are attached to the arthroscopic device, enabling spatial and tactile sensory information to be recorded during usage of the device.

Software

The software architecture consist of two main parts. An integration layer, responsible for sensor acquisitions, data synchronisation as well as persistence and a visualisation layer responsible for displaying the on-going procedure in a virtual 3D environment.

The integration layer is implemented in C++ and makes use of the ZED Software Development Kit (SDK) in order to fetch pose data from the ZED mini camera. Sensor data from the 6 DOF force sensor is retrieved using the ATIDAQ C library from ATI Industrial Automation. The application is configured to continuously transmit data over a network connection for e.g. visualisation purposes. Furthermore, the application can be configured to persist pose and force data to the hard-drive for later processing. The sampling rate is 24 Hz. Due to the requirements of the NI and ZED software used, the application must run on a Windows PC equipped with a CUDA-enabled GPU.

The visualisation layer is implemented using web technologies, enabling clients to view the procedure without any prior software requirements other than a regular web-browser. WebGL, a cross-platform Javascript API for rendering 3D graphics, is used to render the 3D visuals as seen in Fig. 4. In particular, the Javascript library *three.js* is used to simplify interaction with the WebGL API.

Communication between the client and the integration layer is facilitated using Websockets, which is a bi-directional communication protocol supported by all modern browsers. The integration layer acts as a server, and transmits a continuous stream of pose and force/torque data. This information is used to update the 3D scene and display sensor data.

POSITION ACCURACY EXPERIMENT

Position accuracy of the arthroscopic tracker system was tested in an evaluation experiment. The arthroscopic tracker was attached to the end effector of a Kuka LBR Med 14 R820 (Kuka AG, Germany) collaborative robot, and the position was compared with the arthroscopic tracker. The pose repeatability of the LBR Med 14 R820 is ±0.15 mm according to ISO 9283.

1. Arthrex AR 10000 Hook Probe
2. DIN912 M3X10 bolt (x 3)
3. 3D-printed tool adapter
4. ZED Mini stereo camera/IMU
5. DIN912 M3X12 bolt (x 4)
6. 3D-printed handle
7. DIN912 M2x10 bolt (x 2)
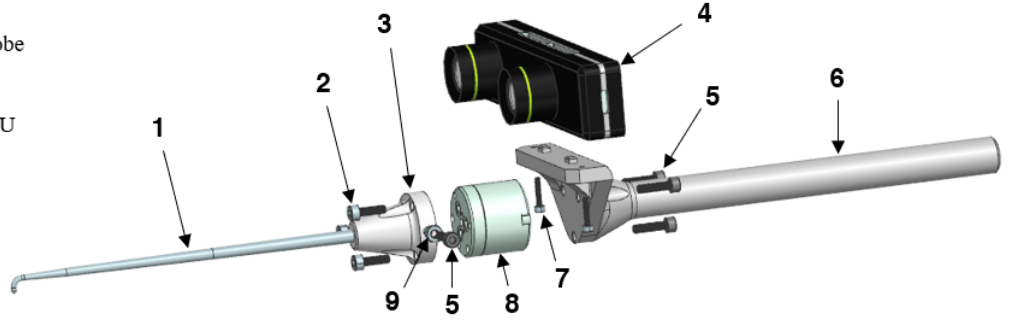8. ATI Nano25 F/T sensor
9. DIN934 M3 nut

Fig. 3: Exploded view of arthroscopic tracker assembly, with bill of materials and components.
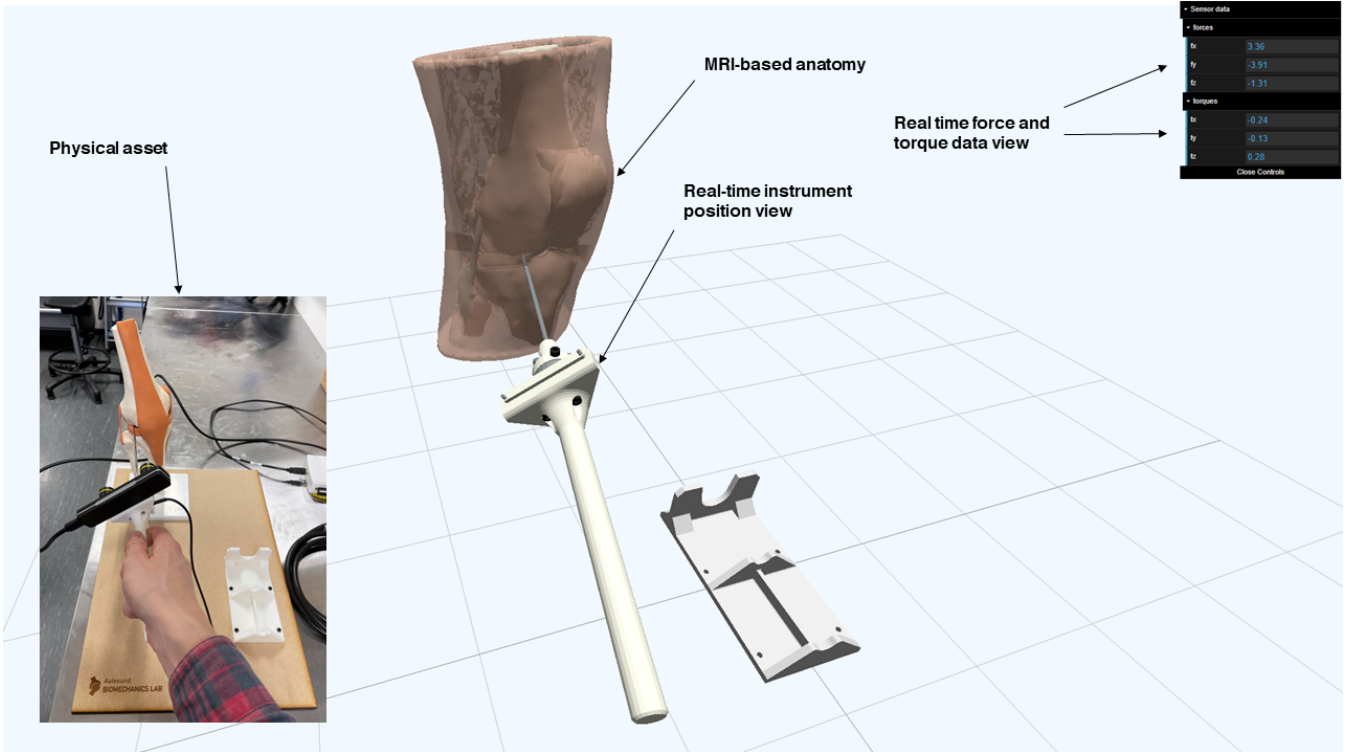

Fig. 4: The visualization layer of the software architecture was facilitated using Websockets, enabling remote real-time visualization of the instrument position and force/torque data.

With the arthroscopic tracker attached, the robot end effector was set to eight random positions within a work space of 250x250x250 mm. Translation was performed along one Cartesian axis at the time. Reference objects were set up in the background to provide reference for the camera.

The differences between the robot end effector and arthroscopic tracker positions were categorized into translation error, position drift, and position error. Translation error was taken as the difference in position just before and right after movement. Position drift was taken as the difference in position readings between movements, typically over 1–2 minutes. The position error was taken as the accumulated error from the translation and drift errors. The root mean square error (RMSE) was calculated, and is presented in Table I.

TABLE I: Root mean square error of translation, drift and position for the arthroscopic tracker. Units are in millimeters.

RMSE	x	y	z	Total
Translation	5.59	6.73	12.00	14.85
Position drift	0.44	1.71	0.73	1.91
Position	5.75	7.63	12.33	12.60

INSTRUMENT TRAJECTORY MAP

As stated in the introduction, instrument pose data combined with interaction forces can be presented in an instrument trajectory map. This section describes implementation of a script for automatic generation of such a map, as well as an experiment demonstrating post-processed visualization of data collected using the arthroscopic tracker prototype.

A script automatically generating an instrument trajectory map from sampled position and force/torque data was created using MATLAB (Mathworks, USA). The script imports a wavefront OBJ file of the anatomy, and plots the instrument tool-path relative to the anatomical model. Vectors indicate the interaction force exerted at the given position. Colors and vector length indicate the magnitude of the force, where the color red is the highest force sampled during the session, and blue is the lowest. Orientation of the vectors indicate the direction of the interaction force.

The wavefront OBJ anatomical model is loaded and displayed using the read and display obj functions. The interaction force is visualized by drawing the force vector using the synchronized probe tip position as origin, and is realized using the COLORFIELD3 function (Sullivan, 2023). Force/torque sensor bias is compensated by sampling data during two seconds in the start position while the arthroscopic tracker is not moving. The interaction force is presented in the force/torque sensor coordinate system (CSYS).

The probe tip position in the world CSYS is calculated using yaw, pitch, roll angles as described by Lynch and Park (2017). Yaw is taken as the rotation about the x-axis, γ, pitch is taken as the rotation about the y-axis, β, and roll is taken as the rotation about the z-axis, α. The world-, camera/IMU- and probe tip CSYS are shown in Fig. 5. A rotation matrix, $\mathbf{R_w}$, with respect to the world CSYS is then found as

$$\mathbf{R_w}(\alpha, \beta, \gamma) = \text{Rot}(\alpha)\text{Rot}(\beta)\text{Rot}(\gamma)I$$

$$= \begin{bmatrix} c_\alpha c_\beta & c_\alpha s_\beta s_\gamma - s_\alpha c_\gamma & c_\alpha s_\beta s_\gamma + s_\alpha c_\gamma \\ s_\alpha c_\beta & s_\alpha s_\beta s_\gamma + c_\alpha c_\gamma & s_\alpha s_\beta c_\gamma - c_\alpha s_\gamma \\ -s_\beta & c_\beta s_\gamma & c_\beta c_\gamma \end{bmatrix}, \quad (1)$$

where s and c are sine and cosine respectively. A homogeneous representation of the position vector, $\mathbf{p_w^{\text{camera}}}$, from the world CSYS to the camera/IMU CSYS (left eye of the ZED mini) is taken as

$$\mathbf{p_w^{\text{camera}}} = \begin{bmatrix} x_w^{\text{camera}} \\ y_w^{\text{camera}} \\ z_w^{\text{camera}} \\ 1 \end{bmatrix}. \quad (2)$$

As such, a 4x4 homogeneous transformation matrix, $\mathbf{T_{w,c}}$, from the camera CSYS to the world CSYS, is found as

$$\mathbf{T_{w,c}}(x_w^{\text{camera}}, y_w^{\text{camera}}, z_w^{\text{camera}}, \alpha, \beta, \gamma)$$

$$= \begin{bmatrix} c_\alpha c_\beta & c_\alpha s_\beta s_\gamma - s_\alpha c_\gamma & c_\alpha s_\beta s_\gamma + s_\alpha c_\gamma & x_w^{\text{camera}} \\ s_\alpha c_\beta & s_\alpha s_\beta s_\gamma + c_\alpha c_\gamma & s_\alpha s_\beta c_\gamma - c_\alpha s_\gamma & y_w^{\text{camera}} \\ -s_\beta & c_\beta s_\gamma & c_\beta c_\gamma & z_w^{\text{camera}} \\ 0 & 0 & 0 & 1 \end{bmatrix}. \quad (3)$$

The probe tip position vector, $\mathbf{p_c^{\text{probe tip}}}$, in the camera CSYS can then be transformed to the world CSYS using the homogeneous transformation matrix:

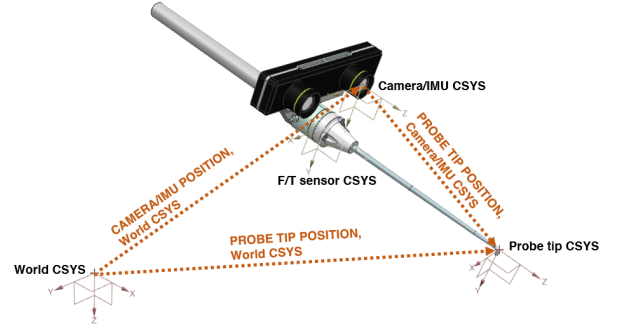$$\mathbf{p_w^{\text{probe tip}}} = \mathbf{T_{w,c}}\mathbf{p_c^{\text{probe tip}}}, \quad (4)$$

Fig. 5: Transformation from probe tip coordinate system to world coordinate system.

where $\mathbf{p_c^{\text{probe tip}}}$ is taken as

$$\mathbf{p_c^{\text{probe tip}}} = \begin{bmatrix} 23.75 \\ 31.75 \\ 150 \\ 1 \end{bmatrix} \mathbf{mm}. \quad (5)$$

Demonstration Experiment

Using the arthroscopic tracker prototype shown in Fig. 2, the probe was moved to the 3B functional knee model, and a series of distal pushes were applied first to the medial meniscus, and then lateral meniscus. The recorded data was saved to a comma separated value (csv) file on the harddrive. The csv file was then imported into MATLAB and the script presented in the previous section was run. The result is shown in Fig. 6.

DISCUSSION

This paper has presented design, implementation and evaluation of an arthroscopic tracker system for intraoperative motion tracking and force registration for use in research and education. The system enables automatic real-time transfer of pose and forces between a physical asset and digital model, as required in arthroscopic digital twins.

The position accuracy of the system was evaluated in an experiment. As can be observed from Table I, the position RMSE between the arthroscopic tracker and robot end effector was 12.60 mm. This is considerably higher than the reported accuracy from the camera/IMU manufacturer (± 1 mm), as well as from another study (Ma et al., 2020) using the same camera/IMU (MSE of 0.99 mm). From observations during testing, we suggest that the accuracy of the system is dependent on the presence of identifiable objects in the background. For example, when a chess patterned object was removed from the background, the RMSE was five times higher than shown in Table I. It is likely that by optimizing light conditions and placement of fiducial markers, a better position accuracy can be achieved. For example could the use of ArUco markers help improve accuracy, as shown by Kam et al. (2018).

Still, considering the achieved position accuracy of 12.6 mm, we conclude that the system is feasible for use in many research and educational applications. Comparing the system with commercial OTS and EMTS, as shown in

TABLE II: Comparison of motion tracking component of presented system compared with other systems. Note that the price does not include F/T sensor or other hardware. ^{a}Depth sensing range as provided by manufacturer (range limited by length of USB cable). ^{b}Max frame rate for camera is 60 Hz, and 800 Hz for IMU.

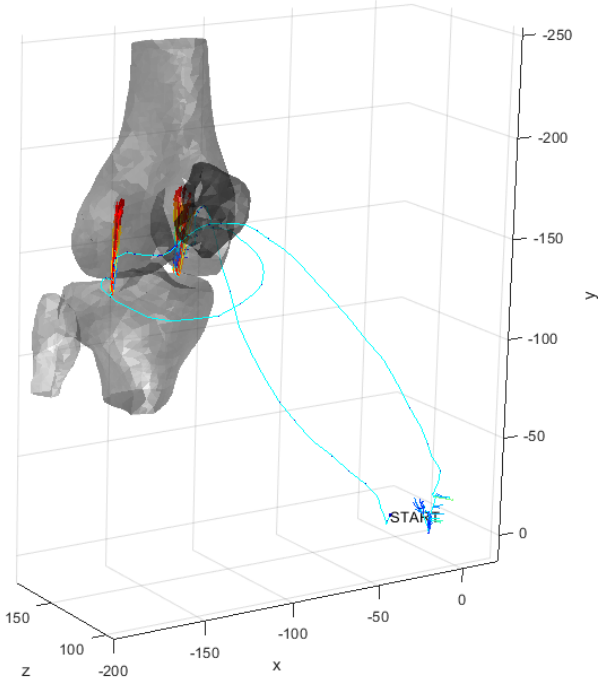|	**Current study**	**VISS**	**OTS**	**EMTS**
Position accuracy	12.6 mm	0.99 mm	0.045 mm	2.2 mm
Work space / range	150-15,000 mm^a	12,000 mm	1856x1470x2050 mm	600 mm
Refresh rate	24 Hz	60 / 800 Hz^b	400 Hz	255 Hz
Approximate price	$440	$440	$11,500 - 30,000*	$15,650 - 17,900*
Reference	-	Ma et al. (2020)	Fattori et al. (2021)	Attivissimo et al. (2021)
			*Hosseini (2013)	*Hosseini (2013)

Fig. 6: A post-operative view of the instrument tool-path (in cyan) relative to the anatomical model. Vectors indicate the interaction force exerted at the given position. Colors and vector length indicate the magnitude of the force (red highest), while the orientation of the arrows indicate direction of the force.

Table II, it is clear that the work space is larger, and that the price is lower than for commercial OTS and EMTS. This makes it suitable for arthroscopy training for resident doctors, as the system could provide navigation aids when learning triangulation techniques on plastic models or human cadaveric specimens. Additionally, the system can provide concurrent feedback through its real-time visualization, as well as post-response feedback through the instrument trajectory map, in order to reduce excessive use of force (as discussed by Tang et al., 2005; Golahmadi et al., 2021). However, the accuracy should be improved for haptic research applications.

The instrument trajectory map facilitated by the arthroscopic tracker system serves as a proof-of-concept for a post-operative virtual surgery database. Such a database could for example provide detailed digital transcripts from a series of operations of one type of surgery. With sufficient data available combined with artificial intelligence, this could serve as a research tool that could provide useful insights into the surgical domain.

To expand the system towards an arthroscopic digital twin, the simulation must not only display the instrument pose relative to the patient-specific anatomical model, but interact with it. Simulation frameworks such as the simulation open framework architecture (SOFA) facilitate real-time soft tissue finite element simulations with interaction using haptic devices (Faure et al., 2012). It is feasible to replace user interaction from a haptic device with the presented arthroscopic tracker system, however position accuracy should be enhanced. Patient specific material properties could also be extracted using the synchronized force and pose data in combination with inverse finite element methods (Seyfi et al., 2018) or machine learning methods (Mendizabal et al., 2020).

CONCLUDING REMARKS

This paper has presented implementation and evaluation of an intraoperative arthroscopic tracker system for research and educational use. Motion tracking is achieved using an inertial measurement unit in combination with stereo vision, and force registration is achieved using a force-torque sensor. The system enables automatic pose and force data exchange between a physical asset and a digital model. Preliminary experiments indicate that the system is feasible for use in many research and educational applications, but that position accuracy should be improved.

ACKNOWLEDGMENTS

REFERENCES

Attivissimo, F., Nisio, A. D., Lanzolla, A. M. L. and Ragolia, M. A. (2021), Analysis of Position Estimation Techniques in a Surgical EM Tracking System, *IEEE Sensors Journal* 21(13), 14389–14396.

Aubert, K., Germaneau, A., Rochette, M., Ye, W., Severyns, M., Billot, M., Rigoard, P. and Vendeuvre, T. (2021), Development of Digital Twins to Optimize Trauma Surgery and Postoperative Management. A Case Study Focusing on Tibial Plateau Fracture, *Frontiers in Bioengineering and Biotechnology* 9, 722275.

Bjelland, Ø., Pedersen, M. D., Steinert, M. and Bye, R. T. (2022), Intraoperative Data-Based Haptic Feedback for Arthroscopic Partial Meniscectomy Punch Simulation, *IEEE Access* 10, 107269–107282.

Bjelland, Ø., Rasheed, B., Schaathun, H. G., Pedersen, M. D., Steinert, M., Hellevik, A. I. and Bye, R. T. (2022), Toward a Digital Twin for Arthroscopic Knee Surgery: A Systematic Review, *IEEE Access* 10, 45029–45052.

Chase, J. G., Zhou, C., Knopp, J. L., Shaw, G. M., Näswall, K., Wong, J. H. K., Malinen, S., Moeller, K., Benyo, B., Chiew, Y. S. and Desaive, T. (2021), Digital Twins in Critical Care: What, When, How, Where, Why?, *IFAC-PapersOnLine* 54(15), 310–315.

Corral-Acero, J., Margara, F., Marciniak, M., Rodero, C., Loncaric, F., Feng, Y., Gilbert, A., Fernandes, J. F., Bukhari, H. A., Wajdan, A., Martinez, M. V., Santos, M. S., Shamohammdi, M., Luo, H., Westphal, P., Leeson, P., DiAchille, P., Gurev, V., Mayr, M., Geris, L., Pathmanathan, P., Morrison, T., Cornelussen, R., Prinzen, F., Delhaas, T., Doltra, A., Sitges, M., Vigmond, E. J., Zacur, E., Grau, V., Rodriguez, B., Remme, E. W., Niederer, S., Mortier, P., McLeod, K., Potse, M., Pueyo, E., Bueno-Orovio, A. and Lamata, P. (2020), The 'Digital Twin' to enable the vision of precision cardiology, *European Heart Journal* 41(48), 4556–4564.

Fattori, G., Lomax, A. J., Weber, D. C. and Safai, S. (2021), Technical assessment of the NDI Polaris Vega optical tracking system, *Radiation Oncology* 16(1), 87.

Faure, F., Duriez, C., Delingette, H., Allard, J., Gilles, B., Marchesseau, S., Talbot, H., Courtecuisse, H., Bousquet, G., Peterlik, I. and Cotin, S. (2012), SOFA: A Multi-Model Framework for Interactive Physical Simulation.

Fuller, A., Fan, Z., Day, C. and Barlow, C. (2020), Digital Twin: Enabling Technologies, Challenges and Open Research, *IEEE Access* 8, 108952–108971.

Golahmadi, A. K., Khan, D. Z., Mylonas, G. P. and Marcus, H. J. (2021), Tool-tissue forces in surgery: A systematic review, *Annals of Medicine and Surgery* 65, 102268.

Hernigou, P., Olejnik, R., Safar, A., Martinov, S., Hernigou, J. and Ferre, B. (2021), Digital twins, artificial intelligence, and machine learning technology to identify a real personalized motion axis of the tibiotalar joint for robotics in total ankle arthroplasty, *International Orthopaedics* 45(9), 2209–2217.

Hosseini, Z. (2013), Virtual fluoroscopy system for arthroscopic surgical training. McMaster University.

Hu, X., Liu, H. and Baena, F. R. Y. (2021), Markerless Navigation System for Orthopaedic Knee Surgery: A Proof of Concept Study, *IEEE Access* 9, 64708–64718.

Kam, H. C., Yu, Y. K. and Wong, K. H. (2018), An improvement on ArUco marker for pose tracking using kalman filter, 2018 19th IEEE/ACIS International Conference on Software Engineering, Artificial Intelligence, Networking and Parallel/Distributed Computing (SNPD), pp. 65–69.

Kulseng, C. P. S., Nainamalai, V., Grøvik, E., Geitung, J.-T., Årøen, A. and Gjesdal, K.-I. (2023), Automatic segmentation of human knee anatomy by a convolutional neural network applying a 3D MRI protocol, *BMC Musculoskeletal Disorders* 24(1), 41.

Lauzeral, N., Borzacchiello, D., Kugler, M., George, D., Rémond, Y., Hostettler, A. and Chinesta, F. (2019), A model order reduction approach to create patient-specific mechanical models of human liver in computational medicine applications, *Computer Methods and Programs in Biomedicine* 170, 95–106.

Lynch, K. M. and Park, F. C. (2017), *Modern robotics: mechanics, planning, and control*, Cambridge University Press, Cambridge, UK.

Ma, C., Cui, X., Chen, F., Ma, L., Xin, S. and Liao, H. (2020), Knee arthroscopic navigation using virtual-vision rendering and self-positioning technology, *International Journal of Computer Assisted Radiology and Surgery* 15(3), 467–477. https://doi.org/10.1007/s11548-019-02099-6

Mendizabal, A., Márquez-Neila, P. and Cotin, S. (2020), Simulation of hyperelastic materials in real-time using deep learning, *Medical Image Analysis* 59, 101569.

Nazari, A. A., Janabi-Sharifi, F. and Zareinia, K. (2021), Image-Based Force Estimation in Medical Applications: A Review, *IEEE Sensors Journal* 21(7), 8805–8830.

Seyfi, B., Fatouraee, N. and Imeni, M. (2018), Mechanical modeling and characterization of meniscus tissue using flat punch indentation and inverse finite element method, *Journal of the Mechanical Behavior of Biomedical Materials* 77, 337–346.

Song, A. and Fu, L. (2019), Multi-dimensional force sensor for haptic interaction: a review, *Virtual Reality & Intelligent Hardware* 1(2), 121–135.

Sullivan, M. (2023), COLORVFIELD3 colored 3d vector field plotter. https://se.mathworks.com/matlabcentral/fileexchange/17755-colorvfield3-colored-3d-vector-field-plotter

Tang, B., Hanna, G. B. and Cuschieri, A. (2005), Analysis of errors enacted by surgical trainees during skills training courses, *Surgery* 138(1), 14–20.

ØYSTEIN BJELLAND was born in Bergen, Norway, in 1991. He received the M.Sc. in mechanical engineering from the Norwegian University of Science and Technology (NTNU), Trondheim, in 2016. He is currently pursuing a Ph.D. degree in engineering cybernetics at NTNU, Ålesund. From 2016 to 2020, he worked as a Mechanical Design Engineer at Clara Venture Labs (formerly Prototech) in Bergen, developing mechatronic systems for oil and gas industry, fuel cell systems for space applications and metal additive manufacturing. Since 2020, he has been a researcher at the Cyber-Physical Systems Lab at NTNU, Ålesund. He is also affiliated with Aalesund Biomechanics Lab and TrollLabs. Current research interests include surgery simulation, haptic feedback and biomechatronics.

LARS IVAR HATLEDAL received the B.Sc. degree in automation, the M.Sc. degree in simulation and visualization, and the Ph.D. degree from NTNU, Ålesund, Norway, in 2013, 2017, and 2021, respectively. From 2013 to 2017, he worked as a part-time Research Assistant with the Intelligent System Laboratory, Department of Ocean Operations and Civil Engineering, NTNU. Still with NTNU, he is currently working as an Associate Professor with the Department of ICT and Natural Sciences. His research interests revolves around software architecture, visualisation and artificial intelligence.

MARTIN STEINERT was born in Dresden, Germany. He received the B.A., M.A., and Ph.D. (Dr.rer.pol) degrees in technology management from the University of Fribourg, Switzerland. He has been an Assistant Professor with the University of Fribourg, Switzerland, a Visiting Scholar at MIT and Stanford University, before changing full time to Stanford University as the Deputy Director of the Center for Design Research (CDR), and an Assistant Professor (Acting) in Mechanical Engineering at Stanford University. Since 2013, he has been a Full Professor of Engineering Design at the Department of Mechanical and Industrial Engineering (MTP), Norwegian University of Science and Technology (NTNU). His research interests focus on the fuzzy front end of new product development and design: optimizing the intersection of engineering design thinking and new product development, mechatronics/sensors, and computer sciences (especially machine learning). A special focus is on conceptual development and alpha prototype generation of high-performance requirements and on experimental tools and setups. As of August 2021, he has more than 200 publications registered in Google Scholar. He has several prizes in both teaching and research. Dr. Steinert has been a member of the Norwegian Academy of Technological Sciences (NTVA) since 2015.

ROBIN T. BYE was born in Ålesund, Norway in 1979 and has been an IEEE Senior Member since 2017. He received the B.Eng. (Hons 1) (2004), M.Eng.Sc. (2005), and Ph.D. (2009) degrees in electrical engineering from the University of New South Wales, Sydney, Australia. Since 2008, he has been working at the Department of ICT and Natural Sciences (IIR), Norwegian University of Science and Technology (NTNU), Ålesund, and became a full professor in 2020. At the department, Prof. Bye heads the undergraduate engineering study programme in Automation and Intelligent Systems as well as the Cyber-Physical Systems Laboratory. His research interests belong to the broad areas of cybernetics, artificial intelligence, neuroengineering, and engineering education. Robin T. Bye was awarded the Goodeve Medal by The Operational Research Society in 2019.